

# HAPS Selection for Hybrid RF/FSO Satellite Networks

Olfa Ben Yahia, Eylem Erdogan, *Senior Member, IEEE*, Gunes Karabulut Kurt, *Senior Member, IEEE*, Ibrahim Altunbas, *Senior Member, IEEE*, Halim Yanikomeroglu, *Fellow, IEEE*

**Abstract**—Non-terrestrial networks have been attracting much interest from the industry and academia. Satellites and high altitude platform station (HAPS) systems are expected to be the key enablers of next-generation wireless networks. In this paper, we introduce a novel downlink satellite communication (SatCom) model where free-space optical (FSO) communication is used between a satellite and HAPS node, and a hybrid FSO/radio-frequency (RF) transmission model is used between the HAPS node and ground station (GS). In the first phase of transmission, the satellite selects the HAPS node that provides the highest signal-to-noise ratio (SNR). In the second phase, the selected HAPS decodes and forwards the signal to the GS. To evaluate the performance of the proposed system, outage probability expressions are derived for exponentiated Weibull (EW) and shadowed-Rician fading models while considering the atmospheric turbulence, stratospheric attenuation, and attenuation due to scattering, path loss, and pointing errors. Furthermore, the impact of aperture averaging, temperature, and wind speed are investigated. Finally, we provide some important guidelines that can be helpful for the design of practical HAPS-aided SatCom.

**Index Terms**—High altitude platform station, hybrid RF/FSO, satellite communication, stratospheric attenuation.

## I. INTRODUCTION

Low-earth orbit (LEO) satellites have promising characteristics including high data rates, wide coverage, distance-independent services, and seamless connectivity for unserved and underserved communities. However, direct links between LEO satellites and ground stations (GSs) are highly susceptible to fading, atmospheric turbulence, path loss due to long transmitter-receiver distances, cloud formations, weather effects [1], and masking effects caused by obstacles and shadowing [2]. Thus, a cooperative-relaying model in which a high altitude platform station (HAPS) aids satellite communication (SatCom) by using decode-and-forward (DF) and amplify-and-forward (AF) relaying strategies can be a promising solution. According to the definition of the International Telecommunication Union (ITU), a HAPS system is a fixed object at an altitude of 20 to 50 km [3]; however, the majority of

recent deployments focused on altitude of 18 to 20 km [1]. In SatCom, a HAPS system can function as an intermediate station to increase coverage and signal-to-noise ratio (SNR) while providing lower latency [1]. Furthermore, due to their small footprint, HAPS systems are suitable for low-latency applications and can deliver wireless communication services directly to terrestrial users [4]. In HAPS-aided SatCom, free-space optical (FSO) communication can be a potent enabler as it provides numerous advantages, including extremely high data rates, and it offers line-of-sight (LOS) connectivity over an unlicensed spectrum [5]. Despite their unique features, FSO links are prone to significant variations in both phase and intensity of the received signal due to fluctuations in the index of refraction turbulence caused by variations in temperature and pressure mostly for longer communication distances [6]. Furthermore, FSO communication is weather-dependent and highly affected by turbulence-induced fading and attenuation. More precisely, FSO links may be significantly degraded by fog and snow, whereas attenuation due to rain may be negligible [7]. Performance analyses of FSO communication have been reported in the literature using Log-normal, Gamma-Gamma, double Gamma-Gamma, and Málaga fading channels. Empirical studies, for their part, have proven that the exponentiated Weibull (EW) fading can be the best fit for different aperture sizes in all weather conditions, especially when aperture averaging is used, where the scintillation is spatially averaged over the aperture to mitigate the effects of atmospheric turbulence and improve the overall performance [8], [9]. Like aperture averaging, spatial diversity can be established between satellites and HAPS systems to provide reliable communication and mitigate the impact of atmospheric turbulence [9].

Another way of reducing the effects of atmospheric turbulence is to incorporate a radio-frequency (RF) link in parallel with the FSO link to benefit from the complementary characteristics. Such hybrid RF/FSO communication can reap all the benefits of RF and FSO communication while minimizing adverse weather-dependent effects. In the literature, two methods of hybrid RF/FSO communication have been reported: soft switching and hard switching [10]. In hard switching, which is more practical, only one link might be active at a time. In this method, the FSO link is active initially, and the RF link acts as a backup should the FSO become unavailable. In the case of soft switching, there is a simultaneous transmission of both links depending on their availability. Hybrid RF/FSO communication has been studied from different perspectives and in various scenarios in [11], [12], [13]. Furthermore, the

O. Ben Yahia, G. Karabulut Kurt and I. Altunbas are with the Department of Electronics and Communication Engineering, Istanbul Technical University, Istanbul, Turkey, (e-mails: {yahiao17, gkurt, ibraltunbas}@itu.edu.tr).

E. Erdogan is with the Department of Electrical and Electronics Engineering, Istanbul Medeniyet University, Istanbul, Turkey, (e-mail: eylem.erdogan@medeniyet.edu.tr).

G. Karabulut Kurt is also with the Department of Electrical Engineering, Polytechnique Montréal, Montréal, QC, Canada (e-mail: gunes.kurt@polymtl.ca).

H. Yanikomeroglu is with the Department of Systems and Computer Engineering, Carleton University, Ottawa, ON, Canada, (e-mail: halim@sce.carleton.ca).

authors in [14] and [15] proposed a parallel transmission of the same information through RF and FSO links, while considering different diversity-combining techniques.

The use of HAPS systems in hybrid RF/FSO communication has also been studied in the literature. In [16], the authors proposed a hybrid scheme for downlink SatCom using a HAPS node as an intermediate terminal between an LEO satellite and GS. In so doing, they derived the average symbol error probability (ASEP) while considering DF relaying and a backup RF channel in the second hop. More recently, in [17], the authors compared a single-hop hybrid RF/FSO SatCom with a dual-hop hybrid RF/FSO communication by using a HAPS node for the uplink. Their results showed that the hybrid RF/FSO outperforms the FSO systems and that the use of the HAPS node improves the performance of uplink SatCom. Our work in this paper differs from these studies by considering a HAPS-assisted SatCom model where the HAPS with the best channel characteristics transmits the information to the GS by using hybrid RF/FSO communication. More precisely, the major contributions of this paper are summarized as follows:

- We propose a novel model for downlink optical SatCom where the best HAPS node with the best channel characteristics is selected.
- To guarantee reliable communication, we consider FSO communication between the satellite and HAPS systems, and hybrid RF-FSO communication is adopted between the HAPS systems and GS.
- We introduce a novel stratospheric attenuation model for satellite-HAPS communication. Furthermore, for different weather conditions, we consider the effects of atmospheric turbulence, attenuation resulting from scattering, path loss, and pointing errors to provide realistic modeling for the proposed setup.
- We investigate the effects of temperature and consider an aperture averaging technique to reduce fluctuations due to turbulence-induced fading and to mitigate the performance degrading-effect of pointing errors.
- We derive the outage probability expressions and validate them with Monte Carlo (MC) simulations. We also provide some important design guidelines that can be helpful in the design of downlink SatCom systems.

This paper is organized as follows: The signal and system model are outlined in Section II. The mathematical expressions of outage probability are derived in Section III. In Section IV, numerical results are presented and discussed, followed by design guidelines. Finally, the conclusion is provided in Section V.

## II. SIGNAL AND SYSTEM MODEL

We consider a dual-hop hybrid SatCom system where an LEO satellite ( $S$ ) seeks to communicate with a GS ( $G$ ) through the best intermediate HAPS ( $H$ ) node, as depicted in Fig. 1. A direct link between  $S$  and  $G$  is unavailable due to atmospheric attenuation between them. In this model,  $H$  acts as a DF relay node and transmits its information using parallel RF and FSO links. In the first phase of the communication,  $S$  selects the HAPS denoted by ( $H_j$ ) that can provide the best

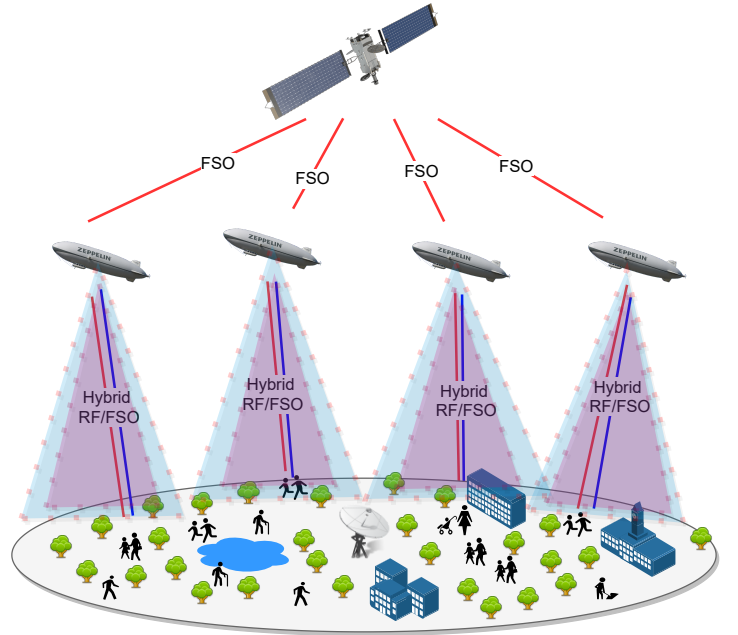


Fig. 1. Illustration of the HAPS node selection for hybrid RF/FSO SatCom.

channel characteristics among  $N$  HAPS to improve the overall performance. In the second phase,  $H_j$  decodes the  $S$  signal and forwards it to  $G$  using hybrid RF/FSO communication. At the ground level, selection combining (SC) is adopted to maximize the utilization of the channel spectrum and to enhance the system as it outputs an SNR equal to the maximum SNR of the two RF and FSO branches [15]. In this setup, the FSO links follow exponentiated Weibull (EW) fading, whereas the RF link is modeled with the shadowed-Rician distribution. Table I summarizes all the parameters used in the paper.

### A. HAPS Selection and Satellite-HAPS Communication

1) *Stratospheric Attenuation*: The idea behind employing a HAPS system is its appealing quasi-stationary position, which avoids the introduction of the Doppler shift. In fact, in addition to its low costs and faster services, at the HAPS level, there are no clouds, which means clean solar energy without atmospheric pollution [18]. However, for long-distance communication, the possibility of volcanic eruptions and resulting aerosol emissions needs to be considered, given that such aerosols can penetrate the stratosphere [19]. Moreover, stratospheric attenuation caused by molecular absorption and scattering by droplets can take place [20]. Considering the stratospheric conditions, polar clouds can cause temperature differences between HAPS and satellite, and this can result in fluctuations in the optical beam. In optical communication, the stratospheric attenuation can be modeled with Beer-Lambert law as follows:

$$I_{SH_j}^l = \exp(-\Psi_{SH_j} L_{SH_j}), \quad (1)$$

where  $\Psi_{SH_j}$  represents the attenuation factor between the satellite and the HAPS systems, and  $L_{SH_j}$  is the propagation distance between  $S$  and  $H_j$  [10]. In Table II, we present

TABLE I  
LIST OF PARAMETERS

Parameter	Definition
$N$	Number of HAPS systems
$L$	Propagation distance
$\xi$	Zenith angle
$D_G$	Hard receiver aperture diameter
$\Theta$	Elevation angle
$u$	RMS wind speed
$h_E$	Height of the GS above mean sea level
$h$	Altitude
$\mathcal{H}$	Altitude of the satellite
$h_H$	Altitude of the HAPS node
$\lambda$	Wavelength
$\alpha, \beta$	Shape parameters of the EW fading
$\eta$	Fading severity parameter of the EW fading
$K$	Optical wave number
$V$	Visibility
$\mathcal{N}$	Cloud number concentration
$\omega$	Geometrical attenuation coefficient
$\Psi$	Stratospheric attenuation coefficient
$\mathcal{L}_W$	Liquid water content
$\sigma_R^2$	Rytov variance
$C_n^2$	Refractive index constant
$\sigma_I^2$	Scintillation index
$\sigma_s$	Jitter standard deviation
$\mathcal{F}$	Path loss
$m$	Nakagami-m fading severity parameter
$\theta$	Transmit divergence angle
$\varphi_{rain}$	Rain attenuation coefficient
$\varphi_{oxy}$	Oxygen attenuation coefficient
$\mathcal{R}$	Rain rate
$n_f$	Noise figure
$T$	Temperature
$B$	Bandwidth
$\gamma_{th}$	Predefined threshold for acceptable communication quality

TABLE II  
STRATOSPHERIC ATTENUATION COEFFICIENT FOR DIFFERENT  
STRATOSPHERIC AEROSOL MODELS AT  $\lambda_{FSO} = 1550$  NM FOR HAPS  
ALTITUDE 19 KM.

Stratospheric aerosol model	Attenuation coefficient $\Psi$ (km <sup>-1</sup> )
Extreme volcanic	$2 \times 10^{-1}$
High volcanic	$5 \times 10^{-2}$
Moderate volcanic	$8 \times 10^{-3}$
Background volcanic	$10^{-4}$

stratospheric aerosol models for different levels of volcanic activity at a specific optical wavelength  $\lambda_{FSO} = 1550$  nm [20].

2) *Stratospheric Turbulence-Induced Fading*: Considering the communication between  $S$  and  $H$ , stratospheric turbulence-induced fading can be caused by non-static stratospheric winds and temperature variations due to altitude and pressure. By considering stratospheric attenuation and stratospheric turbulence-induced fading, the received signal at the  $H_j$  can be expressed as follows:

$$y_{SH_j} = \zeta \sqrt{P_S} I_{SH_j} x_S + n_H, \quad (2)$$

where  $0 \leq \zeta \leq 1$  is the optical-to-electrical conversion coefficient,  $P_S$  is the transmit power of  $S$ ,  $I_{SH_j}$  represents the irradiance of the FSO channel which can be expressed as  $I_{SH_j} = I_{SH_j}^l I_{SH_j}^s$ , where  $I_{SH_j}^s$  denotes the stratospheric

turbulence,  $x_S$  denotes the transmitted signal, and  $n_H$  is the zero-mean additive white Gaussian noise (AWGN) with one-sided power spectral density  $N_0$ . With respect to (2), the instantaneous received SNR at  $H_j$  can be expressed as follows:

$$\gamma_{SH_j} = \frac{\zeta P_S I_{SH_j}^2}{N_0} = \bar{\gamma}_{SH_j} I_{SH_j}^2, \quad (3)$$

where  $\bar{\gamma}_{SH_j} = \frac{\zeta P_S}{N_0}$  is the average SNR with  $\mathbb{E}[I_{SH_j}^2] = 1$ .

In this setup, the HAPS selection is based on the satellite-HAPS channel quality, where the HAPS node with the best channel quality among  $N$  HAPS is selected to maximize the instantaneous SNR between  $S$  and  $H$  as follows:

$$J = \arg \max_{j=1, \dots, N} [\gamma_{SH_j}], \quad (4)$$

where  $1 \leq j \leq N$  shows the HAPS index. Considering the EW fading, the cumulative distribution function (CDF) of  $\gamma_{SH_j}$  can be given as follows [8]:

$$F_{\gamma_{SH_j}}(\gamma) = \prod_{j=1}^N \left( 1 - \exp \left[ - \left( \frac{\gamma}{\bar{\gamma}_{SH_j} (I_{SH_j}^l \eta_{SH_j})^2} \right)^{\frac{\beta_{SH_j}}{2}} \right] \right)^{\alpha_{SH_j}}, \quad (5)$$

where  $\eta_{SH_j}$  is the scale parameter,  $\alpha_{SH_j}$ , and  $\beta_{SH_j}$  present the shape parameters which are directly related to the atmosphere and the scintillation index. These parameters can be expressed as follows [21]:

$$\begin{aligned} \alpha_{SH_j} &= \frac{7.220 \times \sigma_{I_{SH_j}}^{2/3}}{\Gamma(2.487 \sigma_{I_{SH_j}}^{2/6} - 0.104)}, \\ \beta_{SH_j} &= 1.012 \left( \alpha_{SH_j} \sigma_{I_{SH_j}}^2 \right)^{-13/25} + 0.142, \\ \eta_{SH_j} &= \frac{1}{\alpha_{SH_j} \Gamma(1 + 1/\beta_{SH_j}) \mathfrak{g}_1(\alpha_{SH_j}, \beta_{SH_j})}, \end{aligned} \quad (6)$$

where  $\Gamma(\cdot)$  indicates the Gamma function and  $\mathfrak{g}_1(\alpha_{SH_j}, \beta_{SH_j})$  is  $\alpha_{SH_j}$  and  $\beta_{SH_j}$  dependent constant variable given by [9]

$$\mathfrak{g}_1(\alpha_{SH_j}, \beta_{SH_j}) = \sum_{k=0}^{\infty} \frac{(-1)^k \Gamma(\alpha_{SH_j})}{k!(k+1)^{1+1/\beta_{SH_j}} \Gamma(\alpha_{SH_j} - k)}, \quad (7)$$

and  $\sigma_{I_{SH_j}}^2$  is the scintillation index, which can be written as follows [6, Sect. (12)]:

$$\sigma_{I_{SH_j}}^2 = \exp \left[ \frac{0.49 \sigma_{R_{SH_j}}^2}{(1 + 1.11 \sigma_{R_{SH_j}}^{12/5})^{7/6}} + \frac{0.51 \sigma_{R_{SH_j}}^2}{(1 + 0.69 \sigma_{R_{SH_j}}^{12/5})^{5/6}} \right] - 1, \quad (8)$$

where  $\sigma_{R_{SH_j}}^2$  denotes the Rytov variance given as follows [6, Sect. (12)]:

$$\sigma_{R_{SH_j}}^2 = 2.25 K^{7/6} \sec^{11/6}(\xi_{SH_j}) \int_{h_H}^{\mathcal{H}} C_{n_{SH_j}}^2(h) (h - h_H)^{5/6} dh. \quad (9)$$

Here,  $K = \frac{2\pi}{\lambda_{FSO}}$  denotes the optical wave number,  $\xi_{SH_j}$  is the zenith angle,  $\mathcal{H}$  stands for the altitude of the satellite,  $h_H$  indicates the height of the selected HAPS above ground level,

and  $C_{n_{SH_j}}^2(h)$  is the refractive-index parameter depending on the altitude  $h$  expressed as follows [22]:

$$C_{n_{SH_j}}^2(h) = 8.148 \times 10^{-56} u_{SH_j}^2 h^{10} \exp(-h/1000) + 2.7 \times 10^{-16} \exp(-h/1500) + C_0 \exp(-h/100), \quad (10)$$

where  $u_{SH_j} = \sqrt{v_{SH_j}^2 + 30.69v_{SH_j} + 348.91}$  represents the root-mean-square (RMS) of the wind speed,  $v_{SH_j}$  is the wind speed in m/s at  $H_j$ , and  $C_0 = 1 \times 10^{-18}$  is the nominal value of  $C_{n_{SH_j}}^2(h)$  at the HAPS node in  $m^{-2/3}$ .

3) *Pointing Error*: For FSO communication, another critical impairment consists of beam-pointing errors, which significantly affect the performance of networks, especially over large distances. Due to vibrations in the transmitter telescope and thermal expansion, a misalignment between the transmitter and receiver can occur. Pointing errors come down to two issues. First, the boresight, which is the fixed displacement between the beam center and center of the detector. Second, jitter, which represents the random offset of the beam center at the detector plane [23]. In the presence of pointing errors, the irradiance of the FSO channel can be expressed as  $I_{SH_j} = I_{SH_j}^l I_{SH_j}^s I_{SH_j}^p$ , where  $I_{SH_j}^p$  indicates the pointing error component. In our model, we will assume zero boresight pointing errors for the link between the  $S$  all instances of  $H$ . Hence, the PDF of  $I_{SH_j}^p$  can be given as follows [24]:

$$f_{I_{SH_j}^p}(I^p) = \frac{g^2 \exp\left(\frac{-s^2}{2\sigma_s^2}\right)}{A_0 g^2} (I^p)^{g^2-1} I_0\left(\frac{s}{\sigma_s^2} \sqrt{\frac{-w_{eq}^2 \ln \frac{I^p}{A_0}}{2}}\right), \quad (11)$$

where the parameter  $g = w_{eq}/(2\sigma_s)$  is the ratio between the equivalent beam  $w_{eq}$  and the jitter standard deviation  $\sigma_s$ , where  $w_{eq}^2 = w_z^2 \sqrt{\pi} \operatorname{erf}(y)/(2ye^{(-y^2)})$ .  $y = \sqrt{\pi/2\varpi}/w_z$  indicates the ratio of the aperture radius  $\varpi$  and the beam-width  $w_z$  at distance  $z$ ,  $w_z = \theta z$  with  $\theta$  is the beam divergence angle, and  $\operatorname{erf}(\cdot)$  indicates the error function. Moreover,  $s$  denotes the boresight, which is considered to be zero in our case. Finally,  $A_0 = [\operatorname{erf}(y)]^2$  defines the gathered optical power for a zero difference between the optical spot center and the detector center, and  $I_0(x)$  defines the modified Bessel function of the first kind with order zero [24].

4) *Aperture Averaging*: For downlink optical communication, when the receiving aperture is lower than the correlation width of irradiance fluctuations, the turbulence-induced signal fluctuations can deteriorate the system performance. Hence, aperture averaging takes place, and increasing the aperture size not only improves the signal level but also reduces the fluctuations in the received signal. More specifically, the aperture size-dependent scintillation index can be given as follows [6, Sect. (12)]:

$$\sigma_{I_{SH_j}}^2 = 8.7k^{7/6} (\mathcal{H} - h_H)^{5/6} \sec^{11/6}(\xi_{SH_j}) \times \Re \left\{ \int_{h_H}^{\mathcal{H}} C_{n_{SH_j}}^2(h) \times \left[ \left( \frac{kD_G^2}{16L_{SH_j}} + i \frac{h - h_H}{\mathcal{H} - h_H} \right)^{5/6} - \left( \frac{kD_G^2}{16L_{SH_j}} \right)^{5/6} \right] \right\} dh, \quad (12)$$

where  $D_G$  is the hard aperture diameter of the HAPS node in m.

## B. HAPS-Ground Station Communication

In the  $H$  to  $G$  communication, we adopt hybrid RF/FSO communication, where both RF and FSO communication can be selected at ground level depending on the channel characteristics. In other words,  $G$  chooses the best link that maximizes the instantaneous SNR between  $H_j$  and  $G$ .

1) *Atmospheric Attenuation*: The main problem in the optical wireless links is attenuation resulting from scattering and absorption. The scattering of optical signals is mainly caused by weather conditions such as clouds, fog, snow, and rain [7].

In optical communication, Mie scattering is considered to be one of the main sources of signal loss in downlink channels operating at frequencies below 375 THz. It affects the signal when the wavelength is equal to the diameter of the particles in the medium. The following formula, which is used to show the effect of Mie scattering, is suitable for ground stations located at altitudes of  $0 < h_E < 5$  km above the mean sea level. First, we calculate the wavelength-dependent empirical coefficients as follows [25]:

$$\begin{aligned} a &= -0.000545\lambda_{FSO}^2 + 0.002\lambda_{FSO} - 0.0038 \\ b &= 0.00628\lambda_{FSO}^2 - 0.0232\lambda_{FSO} + 0.0439 \\ c &= -0.028\lambda_{FSO}^2 + 0.101\lambda_{FSO} - 0.18 \\ d &= -0.228\lambda_{FSO}^3 + 0.922\lambda_{FSO}^2 - 1.26\lambda_{FSO} + 0.719, \end{aligned} \quad (13)$$

where  $h_E$  indicates the altitude of  $G$  above sea level. Then, the extinction ratio can be expressed as follows [25]:

$$\tau = ah_E^3 + bh_E^2 + ch_E + d, \quad (14)$$

and the atmospheric attenuation due to Mie scattering can be given as follows:

$$I_{H_j G}^m = \exp\left(-\frac{\tau}{\sin(\Theta)}\right), \quad (15)$$

where  $\Theta$  is the elevation angle of the GS.

In optical communication, geometrical scattering can also deteriorate the signal in the atmosphere. In geometrical scattering, fog and cloud-induced fading are the primary causes of FSO communication deterioration. To estimate the attenuation based on the visibility range parameters, the well-known Kim's model can be used to define the attenuation coefficient as [7]

$$\omega = \frac{3.91}{V} \left( \frac{\lambda_{FSO}}{550} \right)^{-x}, \quad (16)$$

where  $V$  defines the visibility range in km, and  $x$  implies the particle size coefficient of scattering given by the Kim model as follows:

$$x = \begin{cases} 1.6 & V > 50 \\ 1.3 & 6 < V < 50 \\ 0.16V + 0.34 & 1 < V < 6 \\ V - 0.5 & 0.5 < V < 1 \\ 0 & V < 0.5. \end{cases} \quad (17)$$

In Table III, the visibility and attenuation coefficient parameters are presented for different fog conditions. Based on this model, for different cloud types, the visibility can be given

TABLE III  
ATMOSPHERIC ATTENUATION AND VISIBILITY PARAMETERS FOR  
DIFFERENT ATTENUATION AND VISIBILITY PARAMETERS FOR DIFFERENT  
FOG CONDITIONS AT  $\lambda_{FSO} = 1550\text{NM}$ .

Fog	Visibility $V$ (km)	Attenuation coefficient $\omega$ (dB/km)
Dense	0.05	339.62
Thick	0.20	84.90
Moderate	0.50	33.96
Light	0.77	16.67
Thin	1.90	4.59

TABLE IV  
GEOMETRICAL SCATTERING PARAMETERS FOR VARIOUS TYPES OF  
CLOUDS AT  $\lambda_{FSO} = 1550\text{NM}$ .

Cloud type	$\mathcal{N}$ ( $\text{cm}^{-3}$ )	$\mathcal{LW}$ ( $\text{g/m}^{-3}$ )	$V$ (km)
Cumulus	250	1.0	0.0280
Stratus	250	0.29	0.0626
Stratocumulus	250	0.15	0.0959
Altostratus	400	0.41	0.0369
Nimbostratus	200	0.65	0.0429
Cirrus	0.025	0.06405	64.66
Thin cirrus	0.5	$3.128 \times 10^{-4}$	290.69

by using the liquid water content ( $\mathcal{LW}$ ) and cloud number concentration ( $\mathcal{N}$ ) as follows [26]:

$$V = \frac{1.002}{(\mathcal{LW}\mathcal{N})^{0.6473}}. \quad (18)$$

The corresponding parameters are summarized in Table IV. Accordingly, the geometrical attenuation can be given by using the Beer-Lambert law as  $I_{H_JG}^g = \exp(-\omega L_{H_JG})$  where  $L_{H_JG}$  is the propagation distance between  $H_J$  and  $G$ . Hence, the total atmospheric attenuation at ground level can be expressed by [27]

$$I_{H_JG}^a = I_{H_JG}^m I_{H_JG}^g. \quad (19)$$

Among the different atmospheric effects on the FSO link, rain is the weakest attenuation factor. However, the size of rain droplets increases when the rainfall rate increases, so it may cause refraction and reflection. Considering the FSO communication, the specific rain attenuation coefficient can be expressed on the basis of the rainfall rate  $\mathcal{R}$  (mm/h) as follows [7]:

$$\varphi_{rain}^{FSO} = 1.076\mathcal{R}^{0.67}. \quad (20)$$

Therefore, the rain attenuation can be obtained using the Beer-Lambert law as  $I_{H_JG}^{rain} = \exp(-\varphi_{rain}^{FSO} L_{H_JG})$ . Thus, in the presence of rain, the total attenuation can be considered as  $I_{H_JG}^a = I_{H_JG}^m I_{H_JG}^g I_{H_JG}^{rain}$ .

2) *Atmospheric Turbulence-Induced Fading*: Temperature and pressure gradients can cause variations in the atmosphere's refractive index in the form of eddies causing atmospheric turbulence-induced fading. In the presence of atmospheric turbulence, the instantaneous SNR at  $G$  can be expressed as follows:

$$\gamma_{H_JG}^{FSO} = \frac{\zeta P_{H_J} I_{H_JG}^2}{N_0} = \bar{\gamma}_{H_JG}^{FSO} I_{H_JG}^2, \quad (21)$$

where  $P_{H_J}$  represents the transmit power of the selected HAPS,  $I_{H_JG}$  denotes the FSO channel gain (irradiance), which is given as  $I_{H_JG} = I_{H_JG}^t I_{H_JG}^a$ , where  $I_{H_JG}^t$  indicates the atmospheric turbulence-induced fading. Moreover,  $\bar{\gamma}_{H_JG}^{FSO} = \frac{\zeta P_{H_J}}{N_0}$  is the average FSO SNR of the  $H_J$  to  $G$  link with  $\mathbb{E}[I_{H_JG}^2] = 1$ . Finally, The CDF of  $\gamma_{H_JG}^{FSO}$  can be expressed as in (5) by replacing  $SH_J$  subscript with  $H_JG$ , and the fading severity parameters can be obtained as in (6).

3) *RF Channel*: Let  $x_{H_J}$  denote the transmitted signal of  $H_J$  with power  $P_{H_J}$  through the RF link. The received signal at  $G$  can be expressed as follows:

$$y_{H_JG} = \sqrt{P_{H_J} \mathcal{F}_{H_JG}} f_{H_JG} x_{H_J} + n_G, \quad (22)$$

where  $n_G$  is the zero-mean AWGN with power spectral density  $N_0$ ,  $f_{H_JG}$  is the channel coefficient of the RF link that follows the shadowed-Rician fading, and  $\mathcal{F}_{H_JG}$  is the path-loss model which can be expressed as [10]

$$\mathcal{F}_{H_JG}[\text{dB}] = G_T + G_R - 20 \log_{10} \left( \frac{4\pi L_{H_JG}}{\lambda_{RF}} \right) - \varphi_{oxy} L_{H_JG} - \varphi_{rain}^{RF} L_{H_JG}, \quad (23)$$

where  $G_T$  and  $G_R$  represent the gains of the transmitting and receiving antennas in dB, respectively.  $\lambda_{RF}$  is the RF wavelength,  $\varphi_{oxy}$  and  $\varphi_{rain}^{RF}$  are the RF attenuation coefficients due to the oxygen and rain scattering [28]. In RF communication, the main attenuation factor is rain, where the corresponding attenuation increases linearly in relation to the rate of rainfall. Thus, the rain attenuation coefficient  $\varphi_{rain}^{RF}$  (dB/km) can be expressed as [29]

$$\varphi_{rain}^{RF} = k_r \mathcal{R}^\varrho. \quad (24)$$

The parameters  $k_r$  and  $\varrho$  depend on the channel's wavelength  $\lambda_{RF}$  (GHz) and can be given as follows [29]:

$$k_r = [k_H + k_V + (k_H - k_V) \cos^2 \Theta \cos 2\iota] / 2, \\ \varrho = [k_H \varrho_H + k_V \varrho_V + (k_H \varrho_H - k_V \varrho_V) \cos^2 \Theta \cos 2\iota] / 2k_r, \quad (25)$$

where the constants  $k_H$ ,  $k_V$ ,  $\varrho_H$ , and  $\varrho_V$  are given in [29] and  $\iota$  is the polarization tilt angle [29]. Therefore, with the help of (24), the instantaneous SNR at  $G$  can be written as follows:

$$\gamma_{H_JG}^{RF} = \frac{P_{H_J} \mathcal{F}_{H_JG} |f_{H_JG}|^2}{N_0} = \bar{\gamma}_{H_JG}^{RF} |f_{H_JG}|^2. \quad (26)$$

where  $\bar{\gamma}_{H_JG}^{RF} = \frac{P_{H_J} \mathcal{F}_{H_JG}}{N_0}$  is the average SNR for the RF link between  $H_J$  and  $G$  with  $\mathbb{E}[|f_{H_JG}|^2] = 1$ . Furthermore, the PDF of the received SNR for the RF link is given by [30]

$$f_{\gamma_{H_JG}^{RF}}(\gamma) = \sum_{l=0}^{m-1} \frac{\mu(1-m)_l (-\delta)^l}{(\bar{\gamma}_{H_JG}^{RF})^{l+1} (l!)^2} (\gamma)^l \exp(-\vartheta\gamma), \quad (27)$$

where  $\mu = \frac{1}{2b} \left( \frac{2bm}{2bm+\Omega} \right)^m$ ,  $\delta = \frac{\Omega}{2b(2bm+\Omega)}$ ,  $\vartheta = \frac{\nu-\delta}{\bar{\gamma}_{H_JG}}$ , and  $\nu = \frac{1}{2b}$  with  $m$  is a positive integer representing the Nakagami-m fading parameter of the corresponding link. Furthermore,  $\Omega$  and  $2b$  are the average power of the LOS component and multi-path component, and  $(\cdot)_l$  indicates the Pochhammer symbol.

### C. Impact of the Temperature Variations

The earth's atmosphere extends up to 700 km above ground level and is divided into four distinct layers on the basis of temperature. SatCom can be affected by the thermal noise, which varies with altitude. For our proposed model, we consider the troposphere and stratosphere layers [6, Sect. (1)].

- Troposphere: This layer extends up to 11 km and contains 75% of the earth's atmospheric mass. The maximum air temperature takes place near the ground and decreases up to  $-55^\circ\text{C}$  with an increase of altitude.
- Stratosphere: This layer starts at 20 km and extends up to 48 km. The air temperature level decreases with an increase of the altitude starting from  $-55^\circ\text{C}$ .

We analyze the impact of the thermal noise associated with these layers. We show that the use of the HAPS node improves the system's performance as the link between the satellite and the HAPS node is less affected by the noise. The noise power  $N_0$  can be given as  $N_0 = P_n n_f$ , where  $n_f$  is the noise figure of the receiver and  $P_n$  is given as follows [17]:

$$P_n(\text{dB}) = k + T + B, \quad (28)$$

where  $k = -228.6$  dBW/K/Hz represents the Boltzmann's constant,  $T$  is the system noise temperature in dBK, and  $B$  denotes the noise bandwidth in dBHz. Please note that (28) can be used either for a HAPS node or GS, depending on the temperature.

### III. OUTAGE PROBABILITY

The outage probability (OP) of a communication channel is defined as the probability of the instantaneous SNR falling below a predefined threshold  $\gamma_{th}$ . This can be expressed as follows [31]:

$$\begin{aligned} P_{out} &= \Pr[\gamma_0 \leq \gamma_{th}] \\ &= F_{\gamma_0}(\gamma_{th}), \end{aligned} \quad (29)$$

where  $F_{\gamma_0}(\gamma_{th})$  is the CDF of the end-to-end SNR at  $G$ , which can be given as follows:

$$\gamma_0 = \min(\gamma_{SH_J}, \gamma_{H_JG}), \quad (30)$$

where  $\gamma_{H_JG} = \max(\gamma_{H_JG}^{FSO}, \gamma_{H_JG}^{RF})$  is the output SNR of the SC at  $G$ , and the CDF of the  $\gamma_0$  can be written as follows:

$$\begin{aligned} F_{\gamma_0}(\gamma) &= 1 - \Pr[\gamma_{SH_J} > \gamma] \Pr[\gamma_{H_JG} > \gamma] \\ &= 1 - \left(1 - F_{\gamma_{SH_J}}(\gamma)\right) \left(1 - F_{\gamma_{H_JG}}(\gamma)\right) \\ &= 1 - \left(1 - F_{\gamma_{SH_J}}(\gamma)\right) \left(1 - \left(F_{\gamma_{H_JG}^{FSO}}(\gamma) F_{\gamma_{H_JG}^{RF}}(\gamma)\right)\right), \end{aligned} \quad (31)$$

where  $F_{\gamma_{H_JG}^{FSO}}(\gamma)$  and  $F_{\gamma_{H_JG}^{RF}}(\gamma)$  are the CDF of  $\gamma_{H_JG}^{FSO}$  and  $\gamma_{H_JG}^{RF}$  respectively, given as follows:

$$\begin{aligned} F_{\gamma_{H_JG}^{FSO}}(\gamma) &= \sum_{\rho=0}^{\infty} \binom{\alpha_{H_JG}}{\rho} (-1)^\rho \\ &\times \exp \left[ -\rho \left( \frac{\gamma}{(\eta_{H_JG} I_{H_JG}^a)^2 \bar{\gamma}_{H_JG}^{FSO}} \right)^{\frac{\beta_{H_JG}}{2}} \right], \end{aligned} \quad (32)$$

$$\begin{aligned} F_{\gamma_{H_JG}^{RF}}(\gamma) &= 1 - \sum_{l=0}^{m-1} \sum_{q=0}^l \frac{\mu(1-m)_l (-\delta)^l}{q! \vartheta^{l-q+1} (\bar{\gamma}_{H_JG}^{RF})^{l+1} l!} \\ &\times (\gamma)^q \exp(-\vartheta \gamma). \end{aligned} \quad (33)$$

Furthermore,  $F_{\gamma_{SH_J}}(\gamma)$  is the CDF of  $\gamma_{SH_J}$ , which can be expressed as given in (5) in the absence of pointing errors. However, in the presence of pointing errors,  $F_{\gamma_{SH_J}}(\gamma)$  can be given as follows [23]:

$$\begin{aligned} F_{\gamma_{SH_J}}(\gamma) &= \prod_{j=1}^N \left( \frac{\alpha_{SH_j} g^2}{\beta_{SH_j}} \left( \frac{1}{\eta_{SH_j} A_0} \sqrt{\frac{\gamma}{\bar{\gamma}_{SH_j} (I_{SH_j}^l)^2}} \right)^{g^2} \right. \\ &\times \left. \sum_{i=0}^{\infty} T_2(i) G_{2,3}^{2,1} \left( T_3(i) \left| \begin{matrix} 1 - T_1, 1 \\ 0, 1 - T_1, -T_1 \end{matrix} \right. \right) \right), \end{aligned} \quad (34)$$

where  $G_{p,q}^{m,n}(x | a_1, \dots, a_p; b_1, \dots, b_q)$  denotes the Meijer G-function [32, eqn. 07.34.02.0001.01],  $T_1 = g^2/\beta_{SH_j}$ ,  $T_2(i) = (-1)^i \Gamma(\alpha_{SH_j}) / [i! \Gamma(\alpha_{SH_j} - i) (1+i)^{1-T_1}]$ , and  $T_3(i) = (1+i) \left( \frac{1}{\eta_{SH_j} A_0} \sqrt{\frac{\gamma}{\bar{\gamma}_{SH_j} (I_{SH_j}^l)^2}} \right)^{\beta_{SH_j}}$ .

By substituting (32), and (33) into (31), then into (29), the final expression of the OP can be obtained as can be seen at the top of the next page.

### IV. NUMERICAL RESULTS AND DISCUSSIONS

In this section, we first validate the theoretical results with the MC simulations. Then, we evaluate the OP of our system model under different weather conditions. In the simulations, the effects of aperture averaging, pointing errors, wind speed, and different levels of thermal noise are investigated in terms of outage probability. Furthermore, we assume that all HAPS systems experience the same atmospheric conditions without losing the generality, and we assume equal transmit power at  $S$  and  $H$ . The fading severity parameters for the RF link, which is modeled as a shadowed-Rician fading channel, are simulated depending on different shadowing severity levels: frequent heavy shadowing ( $m = 1.0$ ,  $b = 0.063$ ,  $\Omega = 8.94 \times 10^{-4}$ ), average shadowing ( $m = 10$ ,  $b = 0.126$ ,  $\Omega = 0.835$ ), and infrequent light shadowing ( $m = 19$ ,  $b = 0.158$ ,  $\Omega = 1.29$ ) [30]. In addition, the following rain-rate parameters are set: light rain ( $\mathcal{R} = 2.5$  mm/h), moderate rain ( $\mathcal{R} = 12.5$  mm/h), and heavy rain ( $\mathcal{R} = 25$  mm/h) [10]. Moreover, for the FSO link between  $H_J$  and  $G$ , the atmospheric turbulence parameters are set to ( $\alpha_{H_JG} = 3.3419$ ,  $\beta_{H_JG} = 2.3131$ ,  $\eta_{H_JG} = 0.78693$ ) for  $u_{H_JG} = 21$  m/s, whereas the stratospheric turbulence parameters are set to ( $\alpha_{SH_J} = 1.5825$ ,  $\beta_{SH_J} = 8.9870$ ,  $\eta_{SH_J} = 1.0025$ ) for  $u_{SH_J} = 65$  m/s without aperture averaging. In all simulations, we assume the sky to be homogeneous and the atmospheric attenuation to change in function of altitude. Finally, the OP is plotted relative to the transmit power at a threshold  $\gamma_{th} = 7$  dB. Table V provides the simulation parameters used in the numerical results section.

#### A. Verification of the Theoretical Expressions

In Fig. 2, we observe a validation of the theoretical results with the MC simulations for  $N = 1$ . As we can see, there

$$\begin{aligned}
P_{out}(\gamma_{th}) = & \prod_{j=1}^N \sum_{\rho=0}^{\infty} \binom{\alpha_{SH_j}}{\rho} (-1)^\rho \exp \left( -\rho \left( \frac{\gamma_{th}}{\eta_{SH_j}^2 (P_S (I_{SH_j}^a)^2 / N_0)} \right)^{\frac{\beta_{SH_j}}{2}} \right) + \sum_{p=0}^{\infty} \binom{\mu}{p} (-1)^p \\
& \times \exp \left( -p \left( \frac{\gamma_{th}}{\eta_{H_JG}^2 (P_{H_J} (I_{H_JG}^a)^2 / N_0)} \right)^{\frac{\beta_{H_JG}}{2}} \right) \times \left( 1 - \sum_{l=0}^{m-1} \sum_{q=0}^l \frac{\mu(1-m)_l (-\delta)^l}{q! \vartheta^{l-q+1} (P_{H_J} \mathcal{F}_{H_JG} / N_0)^{l+1} l!} \gamma_{th}^q \exp(-\vartheta \gamma_{th}) \right) \\
& - \left[ \prod_{j=1}^N \sum_{\rho=0}^{\infty} \binom{\alpha_{SH_j}}{\rho} (-1)^\rho \times \exp \left( -\rho \left( \frac{\gamma_{th}}{\eta_{SH_j}^2 (P_S (I_{SH_j}^a)^2 / N_0)} \right)^{\frac{\beta_{SH_j}}{2}} \right) \times \left( 1 - \sum_{l=0}^{m-1} \sum_{q=0}^l \frac{\mu(1-m)_l (-\delta)^l}{q! \vartheta^{l-q+1} (P_{H_J} \mathcal{F}_{H_JG} / N_0)^{l+1} l!} \right. \right. \\
& \left. \left. \times \gamma_{th}^q \exp(-\vartheta \gamma_{th}) \right) \times \sum_{p=0}^{\infty} \binom{\mu}{p} (-1)^p \times \exp \left( -p \left( \frac{\gamma_{th}}{\eta_{H_JG}^2 (P_{H_J} (I_{H_JG}^a)^2 / N_0)} \right)^{\frac{\beta_{H_JG}}{2}} \right) \right]. \quad (35)
\end{aligned}$$

TABLE V  
PARAMETERS OF FSO AND RF LINKS

Satellite-HAPS	
Parameter	Value
Zenith angle ( $\xi_{SH_j}$ )	65°
Wind speed ( $u_{SH_j}$ )	65 m/s
Optical wavelength ( $\lambda_{FSO}$ )	1550 nm
Temperature ( $T$ )	-55 °C
Noise figure ( $n_f$ )	1 dB
Satellite height ( $\mathcal{H}$ )	500 km
HAPS altitude ( $h_H$ )	19 km
Stratospheric attenuation ( $\Psi$ )	$2.15 \times 10^{-1}$
Bandwidth (B)	0.5 GHz
Nominal value ( $C_0$ )	$10^{-18}$
HAPS-GS (FSO)	
Zenith angle ( $\xi_{H_JG}$ )	20°
Wind speed ( $u_{H_JG}$ )	21 m/s
Optical wavelength ( $\lambda_{FSO}$ )	1550 nm
Elevation above sea level ( $h_E$ )	0.8 km
Nominal value ( $C_0$ )	$1.7 \times 10^{-14}$
HAPS-GS (RF)	
RF wavelength ( $\lambda_{RF}$ )	40 GHz
Transmitter gain ( $G_T$ )	45 dB
Receiver gain ( $G_R$ )	45 dB
Polarization tilt angle ( $\iota$ )	45°
Oxygen scattering ( $\varphi_{oxy}$ )	0.1 dB/km [33]
Common Parameters for HAPS-GS RF and FSO	
Bandwidth (B)	0.5 GHz
Temperature ( $T$ )	18 °C
Noise figure ( $n_f$ )	1 dB
Threshold ( $\gamma_{th}$ )	7 dB

is a good agreement with the simulations, which justifies the correctness of our derivations. Furthermore, this is supported by a comparison between direct communication using the FSO link and HAPS-aided SatCom. As the figure indicates, the use of a HAPS as an intermediate node between the satellite and GS improves communication. In fact, the FSO link from the satellite to the HAPS node is not weather-dependent and is less vulnerable to atmospheric attenuation. Moreover, the comparison shows that HAPS-aided hybrid RF/FSO communication outperforms HAPS-aided FSO and HAPS-aided RF. Finally, it is clear from the figure that the outage probability decreases

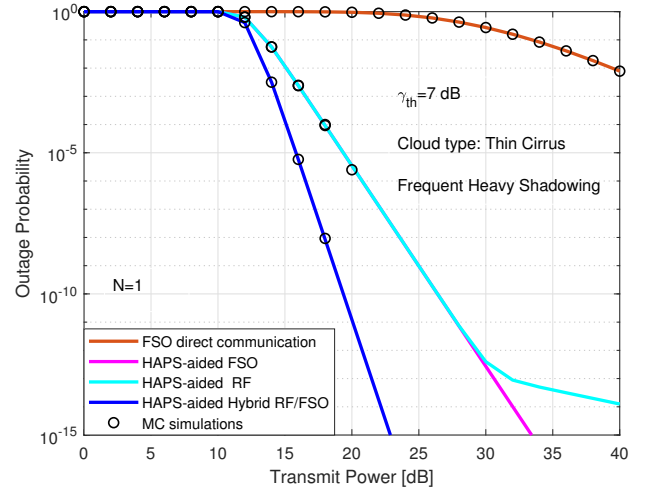


Fig. 2. Outage probability performance under clear weather conditions.

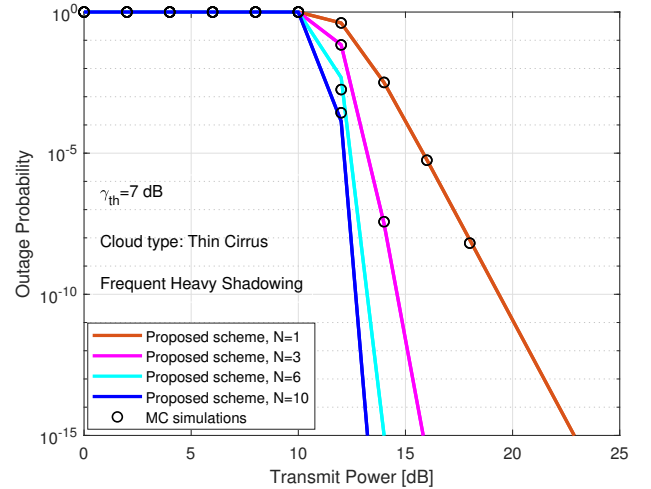


Fig. 3. Outage probability performance for different numbers of HAPS nodes.

when the transmit power increases.

Fig. 3 depicts the outage probability performance for several

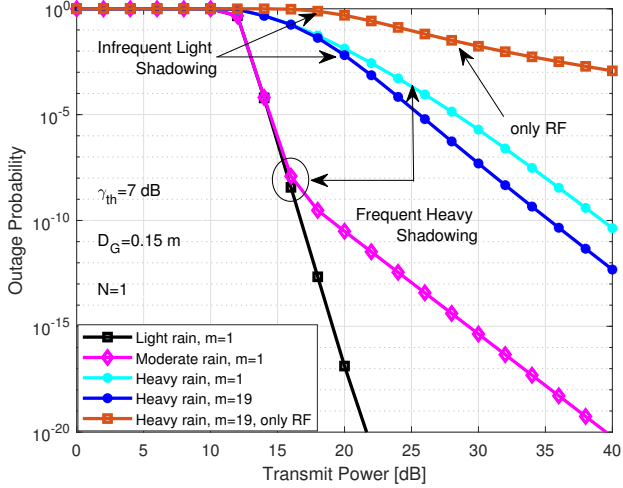


Fig. 4. Outage probability performance of the hybrid RF/FSO under rainy weather conditions.

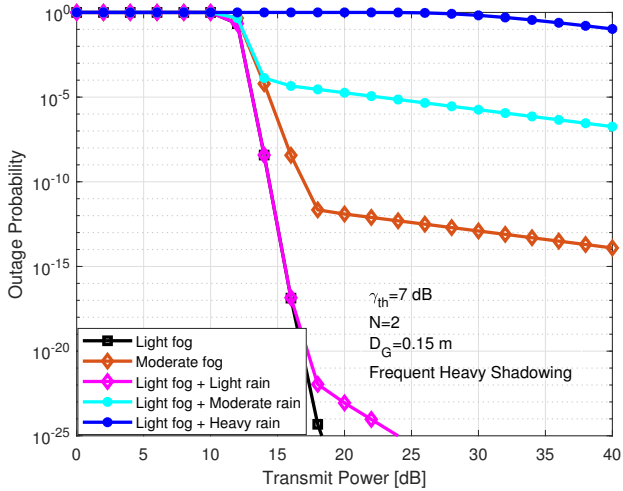


Fig. 5. Outage probability performance of the hybrid RF/FSO under rainy and foggy weather conditions.

HAPS nodes in clear weather conditions. As we can see from the figure, increasing  $N$  improves the overall performance. At an outage of  $10^{-6}$ , we can observe a gain of 4 dB between the curves of  $N = 10$  and  $N = 1$ . Thus, increasing the number of  $N$  enhances the overall performance. Furthermore, the theoretical results are validated with the MC simulations.

In Fig. 4, we can observe the performance of our proposed scheme for different rain levels for  $N = 1$  and with aperture size  $D_G = 0.15$  m. As expected, for a higher rain rate, the overall performance deteriorates as the attenuation level increases. We can see that increasing the severity of the shadowing parameter  $m$  for the RF link improves the overall performance for heavy rain. Moreover, the simulation results show that the RF communication is highly affected by rain and that the hybrid communication relies on the FSO link under rainy conditions.

Fig. 5 shows the effect of foggy and rainy weather on

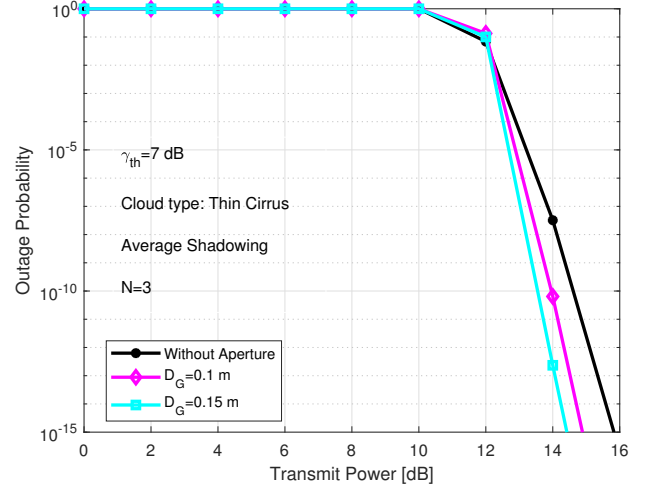


Fig. 6. Outage probability performance of the proposed scheme for various aperture sizes.

the performance of the system for  $N = 2$  and considering an aperture size of  $D_G = 0.15$  m. We first consider light fog, which can be present up to 100 m above ground level. Increasing the thickness of the fog layer from light to moderate deteriorates the performance of the FSO communication, and the RF link becomes dominant for the hybrid communication. Furthermore, in the presence of light fog with all rain levels, the overall performance is highly affected and degraded as both links are affected. The simulation results show that in the presence of light fog and heavy rain, the FSO link is no longer available.

### B. Impact of Aperture Averaging

In this subsection, we analyze the effect of aperture averaging by considering the FSO link for  $N = 3$ . Fig. 6 depicts the hybrid RF/FSO system for different aperture sizes. As the figure indicates, the use of greater aperture sizes increases the gain in terms of transmit power and improves the overall performance by reducing the effect of turbulence-induced fading. Furthermore, with an increase in the aperture size, the energy collected by the receiver beam increase and thus offers more power gain.

### C. Impact of Pointing Error

In Fig. 7, we consider the presence of zero boresight pointing errors for the link from the satellite to the HAPS node. We used different aperture diameter values including  $D_G = 0.15$  m and  $D_G = 0.2$  m, the transmit divergence angle is set as  $\theta = 0.2$  mrad, and  $\sigma_s = 10$  cm for  $N = 1$ . As the link from satellite to HAPS suffers from serious deterioration, it becomes the dominant limitation for communication. Thus, it can be noted that the overall performance is degraded, and this is due to the misalignment between the transmitter and receiver. However, the increase of the aperture size can alleviate this deterioration.

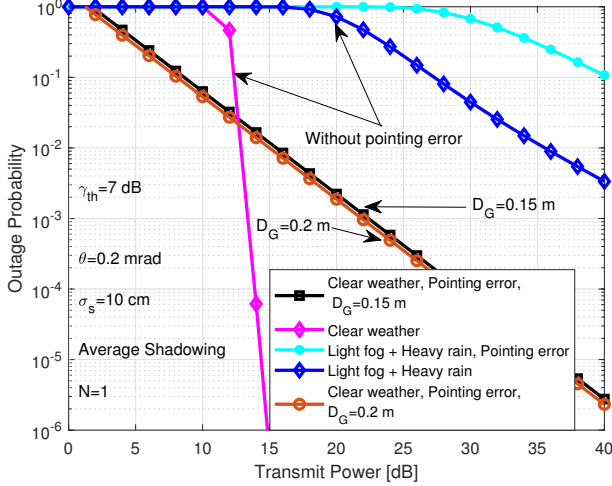


Fig. 7. The impact of pointing errors in terms of outage probability.

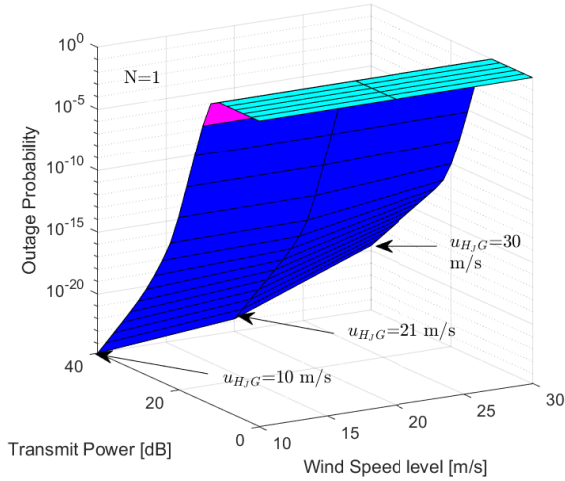


Fig. 8. Outage probability performance of the proposed scheme for different wind speeds.

#### D. Impact of Wind Speed

We also investigate the OP for different wind speed levels at the GS considering one HAPS. For low, moderate and strong wind speed,  $u_{H,J,G}$  is set to  $u_{H,J,G} = 10$  m/s,  $u_{H,J,G} = 21$  m/s, and  $u_{H,J,G} = 30$  m/s respectively for the FSO link between HAPS and GS. As we see in Fig. 8, increasing the wind speed leads to a displacement of the beams, and as the wind speed is directly related to the scintillation index it causes greater atmospheric turbulence and thus deteriorates the overall outage performance. Furthermore, at a lower wind speed  $u_{H,J,G} = 10$  m/s, we can see a power gain compared to  $u_{H,J,G} = 30$  m/s.

#### E. Design Guidelines

In this subsection, we provide guidelines that can help for the design of HAPS-aided SatCom downlink systems.

- The use of HAPS improves SatCom's performance as the link from satellite to HAPS is less affected by the atmospheric turbulence and attenuation.

- The simulations have shown that the FSO channel is slightly affected by rainy weather, whereas the RF link is highly affected, although it remains available. Moreover, the presence of foggy weather deteriorates the FSO communication.
- The zenith angle is directly related to the performance of downlink SatCom. In fact, for lower zenith angle values, we observe lower atmospheric attenuation and this can enhance the overall performance.
- Aperture averaging should be considered as it can mitigate the effect of turbulence-induced fading and improve performance, especially for higher aperture diameter values.
- The misalignment between the transmitter and the receiver caused by pointing errors substantially degrades the overall performance. However, the misalignment can be decreased by using the aperture averaging technique.
- The HAPS selection based on the satellite-HAPS channel quality improves the overall performance.

#### V. CONCLUSION

In this paper, we proposed a new HAPS-assisted downlink SatCom model with hybrid RF/FSO communication. More precisely, in the first phase of transmission, the best HAPS node was selected among multiple HAPS nodes, and then in the second phase we focused on the simultaneous transmission of both RF and FSO links. For the proposed model, the outage probability was derived, and Monte Carlo simulations were provided to validate the accuracy of our analytical results. Furthermore, we considered different weather conditions and investigated the impact of pointing errors, temperature, aperture averaging, and wind speed. The simulations indicated that zero boresight pointing errors lead to severe performance impairments and that the aperture averaging can mitigate the effect of turbulence-induced fading and misalignment caused by pointing errors. Moreover, the HAPS selection based on the satellite-HAPS channel was shown to enhance the overall performance. Finally, guidelines were provided for the design of a HAPS-aided SatCom system.

#### REFERENCES

- [1] M. S. Alam, G. K. Kurt, H. Yanikomeroglu, P. Zhu, and N. D. Dao, "High altitude platform station based super macro base station constellations," *IEEE Commun. Magazine*, vol. 7, no. 1, pp. 103–109, 2021.
- [2] K. Guo, M. Lin, B. Zhang, J.-B. Wang, Y. Wu, W.-P. Zhu, and J. Cheng, "Performance analysis of hybrid satellite-terrestrial cooperative networks with relay selection," *IEEE Trans. on Veh. Technol.*, vol. 69, no. 8, pp. 9053–9067, 2020.
- [3] ITU, "Radio regulations articles." International Telecommunication Union, Recommendation, 2016.
- [4] G. Karabulut Kurt, M. G. Khoshkholgh, S. Alfattani, A. Ibrahim, T. S. J. Darwish, M. S. Alam, H. Yanikomeroglu, and A. Yongacoglu, "A vision and framework for the high altitude platform station (HAPS) networks of the future," *IEEE Communications Surveys Tutorials*, vol. 23, no. 2, pp. 729–779, 2021.
- [5] S. C. Arum, D. Grace, and P. D. Mitchell, "A review of wireless communication using high-altitude platforms for extended coverage and capacity," *Computer Communications*, vol. 157, pp. 232–256, 2020.
- [6] L. C. Andrews and R. L. Phillips, "Laser beam propagation through random media (SPIE Press Monograph)." Bellingham, WA, USA: SPIE, 2005.

- [7] F. Nadeem, V. Kvicera, M. S. Awan, E. Leitgeb, S. S. Muhammad, and G. Kandus, "Weather effects on hybrid FSO/RF communication link," *IEEE Journal on Selected Areas in Commun.*, vol. 27, no. 9, pp. 1687–1697, 2009.
- [8] R. Barrios and F. Dios, "Exponentiated Weibull distribution family under aperture averaging for gaussian beam waves," *Optics Express*, vol. 20, no. 12, pp. 13 055–13 064, 2012.
- [9] E. Erdogan, I. Altunbas, G. K. Kurt, M. Bellemare, G. Lamontagne, and H. Yanikomeroglu, "Site diversity in downlink optical satellite networks through ground station selection," *IEEE Access*, vol. 9, pp. 31 179–31 190, 2021.
- [10] H. Kazemi, M. Uysal, and F. Touati, "Outage analysis of hybrid FSO/RF systems based on finite-state Markov chain modeling," in *Int. Workshop in Optical Wireless Commun. (IWOW)*, pp. 11–15, 2014.
- [11] P. Krishnan, "Performance analysis of hybrid RF/FSO system using BPSK-SIM and DPSK-SIM over Gamma-Gamma turbulence channel with pointing errors for smart city applications," *IEEE Access*, vol. 6, pp. 75 025–75 032, 2018.
- [12] B. Bag, A. Das, I. S. Ansari, A. Prokeš, C. Bose, and A. Chandra, "Performance analysis of hybrid FSO systems using FSO/RF-FSO link adaptation," *IEEE Photon. J.*, vol. 10, no. 3, pp. 1–17, 2018.
- [13] B. Bag, A. Das, C. Bose, and A. Chandra, "Hybrid FSO/RF-FSO systems over generalized Málaga distributed channels with pointing errors," in *European Signal Process. Conf. (EUSIPCO)*, 2019, pp. 1–5.
- [14] M. A. Amirabadi and V. T. Vakili, "A novel hybrid FSO/RF communication system with receive diversity," *Optik*, vol. 184, pp. 293–298, 2019.
- [15] V. Sundharam and S. Johari, "Selection Combining in hybrid RF/FSO systems for IM/DD and heterodyne detection in varying weather conditions," in *Micro-Electronics and Telecom Eng (ICMETE)*, 2018, pp. 286–291.
- [16] R. Swaminathan, S. Sharma, and A. MadhuKumar, "Performance analysis of HAPS-based relaying for hybrid FSO/RF downlink satellite communication," in *Veh. Technol. Conf. (VTC2020-Spring)*, 2020, pp. 1–5.
- [17] R. Swaminathan, S. Sharma, N. Vishwakarma, and A. Madhukumar, "HAPS-based relaying for integrated space-air-ground networks with hybrid FSO/RF communication: A performance analysis," *IEEE Trans. on Aerospace and Electronic Sys.*, vol. 17, pp. 1–17, 2021.
- [18] A. Aragon-Zavala, J. L. Cuevas-Ruiz, and J. A. Delgado-Penín, *High-Altitude Platforms for Wireless Communications*. Wiley Online Library, 2008, vol. 5.
- [19] F. Fidler, M. Knapek, J. Horwath, and W. R. Leeb, "Optical communications for high-altitude platforms," *IEEE J. of Sel. Topics in Quantum Electronics*, vol. 16, no. 5, pp. 1058–1070, 2010.
- [20] D. Giggenbach, R. Purvinskas, M. Werner, and M. Holzbock, "Stratospheric optical inter-platform links for high altitude platforms," in *Int. Commun. Satellite Systems Conf. and Exhibit*, 2002, p. 1910.
- [21] R. Barrios Porras, "Exponentiated Weibull fading channel model in free-space optical communications under atmospheric turbulence." Ph.D. dissertation, Dept. Signal Theory Commun., Univ. Politècnica de Catalunya (UPC), Barcelona, Spain, May 2013.
- [22] ITU, "Propagation data required for the design of Earth-space systems operating between 20 THz and 375 THz." International Telecommunication Union, Recommendation P.1622, 2003.
- [23] Y. Wang, P. Wang, X. Liu, and T. Cao, "On the performance of dual-hop mixed RF/FSO wireless communication system in urban area over aggregated exponentiated Weibull fading channels with pointing errors," *Optics Commun.*, vol. 410, pp. 609–616, 2018.
- [24] F. Yang, J. Cheng, and T. A. Tsiftsis, "Free-space optical communication with nonzero boresight pointing errors," *IEEE Trans. on Commun.*, vol. 62, no. 2, pp. 713–725, 2014.
- [25] ITU, "Prediction methods required for the design of Earth-space systems operating between 20 THz and 375 THz." International Telecommunication Union, Recommendation P.1622, 2003.
- [26] M. S. Awan, E. Leitgeb, B. Hillbrand, F. Nadeem, M. Khan *et al.*, "Cloud attenuations for free-space optical links," in *Int. Workshop on Satellite and Space Commun.* IEEE, 2009, pp. 274–278.
- [27] S. Johari and V. Sundharam, "Performance analysis of IM/DD vs. heterodyne detection techniques of an Earth-satellite FSO link for next generation wireless communication," in *IEEE Malaysia Int. Conf. on Commun. (MICC)*, 2017, pp. 191–196.
- [28] A. Touati, A. Abdaoui, F. Touati, M. Uysal, and A. Bouallegue, "On the effects of combined atmospheric fading and misalignment on the hybrid FSO/RF transmission," *J. of Optical Commun. and Netw.*, vol. 8, no. 10, pp. 715–725, 2016.
- [29] ITU, "Specific attenuation model for rain for use in prediction methods." International Telecommunication Union, Recommendation P.838-1, 2003.
- [30] Y. Ai, A. Mathur, M. Cheffena, M. R. Bhatnagar, and H. Lei, "Physical layer security of hybrid satellite-FSO cooperative systems," *IEEE Photon. J.*, vol. 11, no. 1, pp. 1–14, 2019.
- [31] E. T. Michailidis, N. Nomikos, P. Bithas, D. Vouyioukas, and A. G. Kanatas, "Outage probability of triple-hop mixed RF/FSO/RF stratospheric communication systems," in *IEEE Int. Conf. on Adv. in Satellite and Space Commun. (SPACOMM)*, 2018, pp. 1–6.
- [32] The Wolfram functions site. [Online]. Available: <http://www.wolfram.com>
- [33] A. El Oualkadi, *Trends and Challenges in CMOS Design for Emerging 60 GHz WPAN Applications*. InTech, 2011.